ACS APPLIED MATERIALS & INTERFACES

Research Article

www.acsami.org

Highly Effective Field-Effect Mobility Amorphous InGaZnO TFT Mediated by Directional Silver Nanowire Arrays

Hung-Chuan Liu,[†] Yi-Chun Lai,[†] Chih-Chung Lai,[‡] Bing-Shu Wu,[†] Hsiao-Wen Zan,*[,†] Peichen Yu,*[,†] Yu-Lun Chueh,[‡] and Chuang-Chuang Tsai[†]

[†]Department of Photonics, Institute of Electro-Optical Engineering, National Chiao Tung University, Hsinchu 300, Taiwan

[‡]Department of Materials Science and Engineering, National Tsing Hua University, Hsinchu 300, Taiwan

Supporting Information

ABSTRACT: In this work, we demonstrate sputtered amorphous indium−gallium−zinc oxide thin-film transistors (a-IGZO TFTs) with a record high effective field-effect mobility of 174 cm^2/V s by incorporating silver nanowire (AgNW) arrays to channel electron transport. Compared to the reference counterpart without nanowires, the over 5-fold enhancement in the effective field-effect mobility exhibits clear dependence on the orientation as well as the surface coverage ratio of silver nanowires. Detailed material and device analyses reveal that during the room-temperature IGZO sputtering indium and oxygen diffuse into the nanowire matrix while the nanowire morphology and good contact between IGZO and nanowires are maintained. The unchanged morphology and good interfacial contact lead to high mobility and air-ambient-stable characteristics up to 3 months. Neither hysteresis nor degraded bias stress reliability is observed. The proposed AgNW-mediated a-IGZO TFTs are promising for development of large-scale, flexible, transparent electronics.

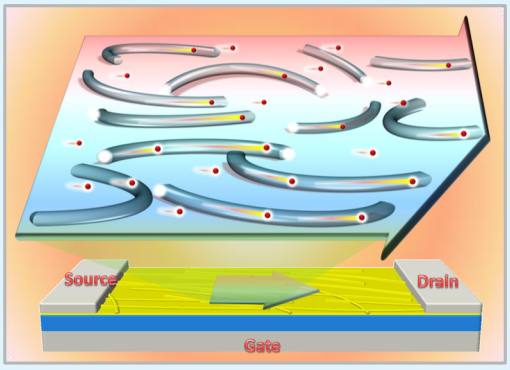

KEYWORDS: *silver nanowire, IGZO, oxide TFT, high mobility*

INTRODUCTION

Amorphous oxide semiconductor (AOS) thin-film transistors (TFTs) have drawn lots of attention due to their low production cost and high mobility. AOS films can be easily deposited using room-temperature magnetron sputtering[1,2] or a solution sol−gel process.[3] For both crystalline (c) and amorphous (a) oxide semiconductors the conduction band is formed by the overlapped s orbital of metal ions.[2] Because the s orbital has no specific directions, the oxide semiconductor can maintain its orbital-overlapped band structure for electron transport even in the amorphous network.[4] Therefore, compared with amorphous hydrogenated silicon (a-Si:H) TFTs, AOS TFTs exhibit relatively high electron mobilities. Currently, the sputtered and sol−gel amorphous indium−gallium−zinc oxide (a-IGZO) TFTs have a typical effective mobility in the range of 10−40 and 1−14 cm^2/V s, respectively.[3,5−8] Together with a large energy band gap (>3 eV) to enable the transparency property, AOS TFTs are promising for developing flexible and transparent electronic devices.[9−11]

Current developments of AOS TFTs have been focused on increasing the effective mobility, i.e., the on-state current, without sacrificing the threshold voltage (V_T) and subthreshold swing (*S.S.*) for low-power operation. Over the past few years, significant progress has been made in sol−gel AOS TFTs by incorporating indium oxide (In_2O_3) nanocrystals (NCs) or carbon nanotubes (CNTs) into sol−gel AOS films. The electron mobilities in sol−gel IZO/In_2O_3, IZO/CNT, and IGZO/CNT TFTs have reached 32.6,[12] 140,[13] and 132 cm^2/V s,[14] respectively. Since the mobility in the pristine sol−gel AOS is rather low, the composite material requires high concentrations of NCs or CNTs without forming nanocrystal boundaries or carrier traps for electron transport.[12,14−16] Still, the relatively high threshold voltage and/or hysteresis characteristics indicate the presence of high defect densities, which temporarily restrict practical applications of sol−gel AOS TFTs. On the other hand, sputtered AOS TFTs generally have lower V_T and *S.S.* than the sol−gel counterparts. Nevertheless, incorporating In_2O_3 nanoparticles into sputtered a-IGZO TFT delivers a much lower effective mobility, ∼5 cm^2/V s,[17] than those of the pristine IGZO and sol−gel IZO/In_2O_3 TFTs.[12] In other words, while sputtered a-IGZO TFTs are widely employed for commercial products, viable solutions to boost their effective mobilities without sacrificing reliability have been scarce.

In this work, we demonstrate sputtered a-IGZO TFTs with a record high effective field-effect mobility μ_{FE} of 174 cm^2/V s by incorporating directional silver nanowire (AgNW) arrays to

Received: September 2, 2014
Accepted: December 8, 2014
Published: December 8, 2014

DOI: 10.1021/am5059316
ACS Appl. Mater. Interfaces 2015, 7, 232−240

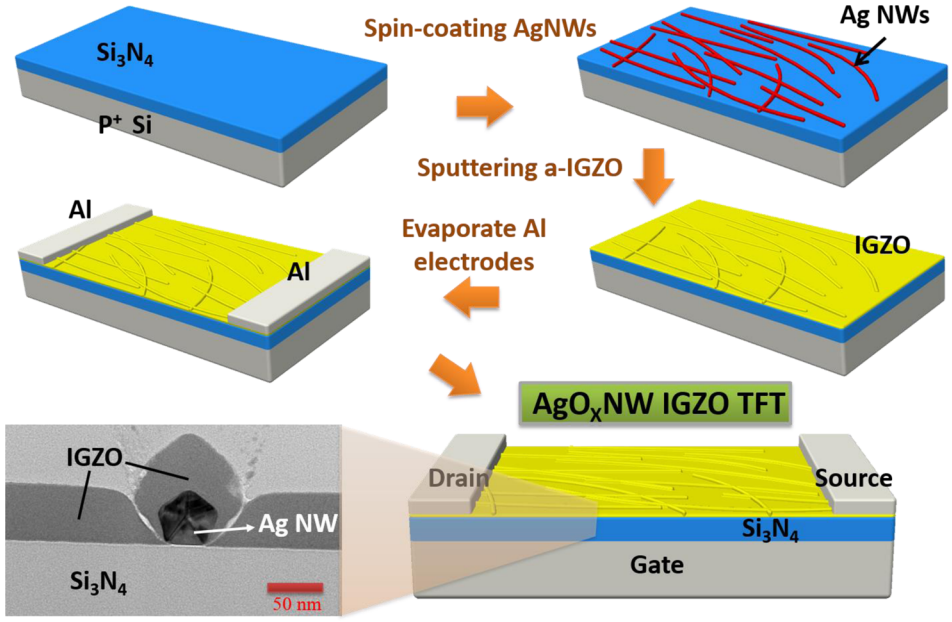

Figure 1. Schematic fabrication process of AgO_xNW a-IGZO TFT. (Inset) TEM image.

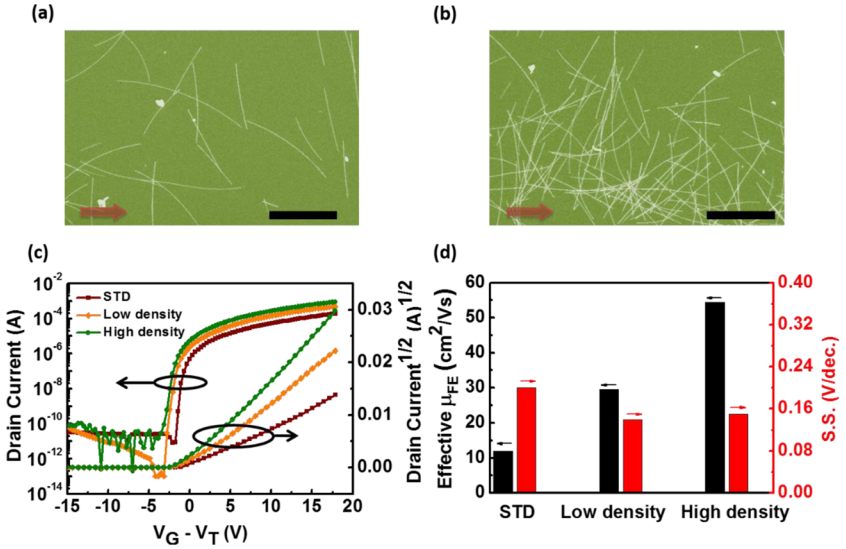

Figure 2. (a and b) SEM images of AgO_xNW a-IGZO TFT with low and high AgO_xNW densities, respectively. Scale bar represents 15 μm. Arrow indicates the direction of current flow from source to drain electrodes. (c) Transfer characteristics of STD a-IGZO TFT and AgO_xNW a-IGZO TFTs with low/high AgO_xNW densities. (d) Effective field-effect mobility and subthreshold swing of the three devices in c are compared.

achieve an over 5-fold enhancement factor over the reference device. While metallic nanowires have been intensively studied as potential candidates for flexible transparent electrodes over the past decade,[18−22] their application in AOS TFTs to serve as an active layer has not been reported. The highly conductive nanowires serve as high-speed bus lines to channel electron transport which greatly improves the effective μ_{FE} without significantly deteriorating V_T and *S.S.* In the proposed devices, the V_T and *S.S.* are around 0.5 and 0.2 V/dec, respectively. Furthermore, controlling the nanowire density and orientation angles can modulate the effective μ_{FE} from 25 to 112 cm^2/V s. On the contrary, elevating the sputtering temperature to 150 °C significantly degrades the effective μ_{FE} to 7 cm^2/V s. High-resolution transmission electron microscopy (TEM) analyses reveal that the room-temperature IGZO sputtering process facilitates indium and oxygen diffusion into the nanowire matrix to form conductive metal oxide compounds (AgO_x with 2−3% In) without changing the nanowire morphology. The good contact between IGZO and nanowires plays a key role to obtain a high effective μ_{FE}. The strong dependence of the effective μ_{FE} on the lateral field further verifies electrons transporting through multiple a-IGZO/AgO_x heterojunctions. Regarding the reliability issue, compared with STD IGZO TFT (without AgOxNW), neither hysteresis nor degraded bias-stress reliability is observed in AgO_xNW a-IGZO TFTs. The superior device characteristics in AgO_xNW IGZO TFTs are stable in the air ambient for over 3 months. The excellent reliability sheds light into the deployment of AgO_xNW-mediated a-IGZO TFTs for large-scale, flexible, transparent electronics with ultralow power consumption. In future works, nanoimprint,[23] nanowire electrospinning,[24] or nanowire contact coating[25] are promising technologies to improve the order of the aligned silver

DOI: 10.1021/am5059316
ACS Appl. Mater. Interfaces 2015, 7, 232−240

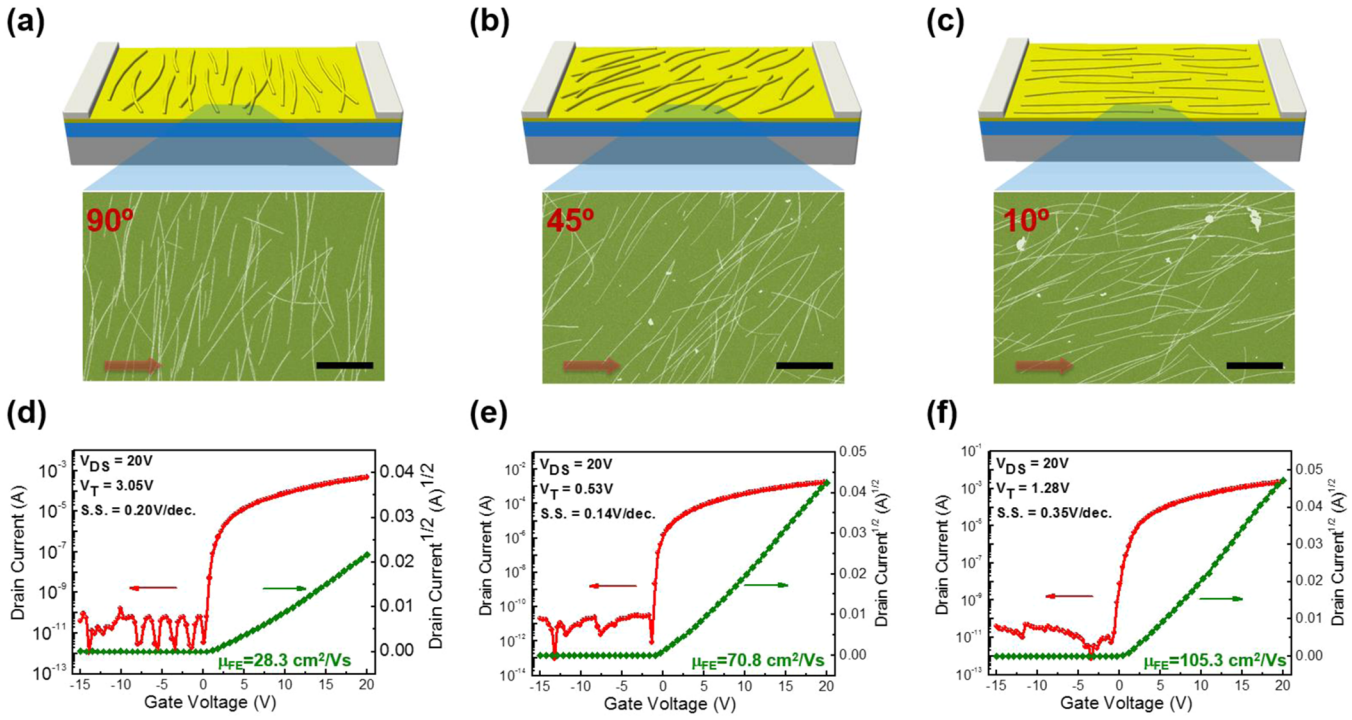

Figure 3. (a, b, and c) Schematic diagrams and SEM images of AgO_xNW a-IGZO TFTs when the angle between the nanowire orientation and the current flow direction is 90°, 45°, and 10°, respectively. Scale bar represents 15 μm. Arrow indicates the direction of current flow from source to drain electrodes. (d, e, and f) Corresponding transfer characteristics of AgO_xNW a-IGZO TFTs with nanowire orientation as 90°, 45°, and 10°, respectively.

nanowire and to scale down the nanowire length as well as the channel length.

EXPERIMENTAL SECTION

The fabrication process of AgO_xNW a-IGZO TFT is schematically illustrated in Figure 1. The p-type heavily doped Si wafer (Addison Engineering Inc.) was prepared as the bottom gate, and the 100 nm thick SiN_x was used as the bottom gate insulator. The capacitance of the SiN_x dielectric is 53.1 nF/cm^2. Silver nanowires (Nanostructured & Amorphous Materials Inc.) suspended in isopropanol (IPA) with a concentration ranging from 0.0625 to 0.125 wt % were deposited onto SiN_x via a blade or spin coating technique. The length and diameter of the nanowires are approximately 10−15 μm and 70−100 nm, respectively. The blade coating process is performed using a blade rod with 7 mm diameter to roll over the substrate.[26] The silver nanowire solution flows through the grooves of the blade and forms the thin liquid film. After the liquid film was volatilized, we heated the substrate at 80 °C for 1 min to avoid the remaining organic solvent. The AgNW network without specific orientations was then formed. For spin-coated AgNWs, we dropped 50 μL of IPA solution with AgNWs on the substrate at a slow spin rate (1000 rpm) for 10 s to avoid agglomeration and then increased the spin rate to 2000 rpm for 40 s for even dispersement of AgNWs. The orientation of aligned AgNWs is affected by the centrifugal force. Hence, AgNWs form a radiative pattern. Choosing TFTs at different locations enabled a rough control for the angle between the orientation of nanowires and the direction of current flow (see Figure S1, Supporting Information). Next, we used radiofrequency sputtering to deposit a 50 nm thick active layer of a-IGZO (Toshima Mfg Co. Ltd., In:Ga:Zn:O = 1:1:1:4)[27,28] onto SiN_x through a shadow mask at room temperature in the argon atmosphere. The channel width was controlled by the width of IGZO pattern as 1000 μm. Then the substrate was annealed at 400 °C for 1 h in a nitrogen furnace. Finally, a 100 nm thick layer of aluminum (Al) was deposited through a shadow mask to form source (S) and drain (D) electrodes, which also defined the channel length as 500 μm. The cross-sectional transmission electron microscope (TEM) image of a nanowire coated with the IGZO thin film is shown in the inset of Figure 1. The cross-sectional scanned electron microscope (SEM) images are also provided in Figures S2a and S2b, Supporting Information.

RESULTS AND DISCUSSION

We first investigate the transfer characteristics of a-IGZO TFT with randomly distributed AgNWs. The randomly distributed nanowire networks are formed by blade coating.[26] SEM images of AgO_xNW a-IGZO TFTs with low and high nanowire densities are shown in Figure 2a and 2b, respectively. Densities are estimated by calculating the surface shield ratio of AgNWs from the SEM images. The corresponding shield ratios are 0.1% in Figure 2a and 27.5% in Figure 2b. The transfer characteristics of the STD and AgO_xNW a-IGZO TFTs with different nanowire densities are plotted in Figure 2c. We note that further increase of the nanowire density results in device shorting between source and drain. The effective field-effect mobility and subthreshold swing of the three devices shown in Figure 2c are extracted and compared in Figure 2d. For STD a-IGZO TFT, the field effect mobility is 12 cm^2/V s. For AgO_xNW a-IGZO TFT, increasing nanowire density leads to an increase of effective μ_{FE} from 29.5 to 54.9 cm^2/V s. The subthreshold swing of the AgO_xNW a-IGZO TFTs is similar to that of the STD a-IGZO TFT, confirming that introduction of AgNWs into the active layer does not significantly degrade the gate control ability. A low subthreshold swing (<0.2 V/dec.) also indicates good interface property with low defect density in the AgO_xNW a-IGZO TFTs. The randomly distributed AgNW network, however, suffers from the uniformity issue. One device may have part of the channel covered by AgNW with a shield ratio as 0.1% (Figure 2a) and the other part covered by a 6% shield ratio (see SEM image in Figure S3, Supporting

DOI: 10.1021/am5059316
ACS Appl. Mater. Interfaces 2015, 7, 232−240

Table 1. Typical Parameters of AgO_xNW a-IGZO TFTs with Different Nanowire Orientations[a]

	nanowire orientation	effective μ_{FE} (cm^2/V s)	V_T (V)	S.S. (V/dec)	on/off ratio
AgO_xNW a-IGZO TFT	90°	26.7 ± 3.9	0.7 ± 0.5	0.16 ± 0.02	10^7−10^8
	45°	76.8 ± 6.8	0.2 ± 0.4	0.19 ± 0.06	10^7−10^8
	10°	114.3 ± 10.2	0.6 ± 0.4	0.21 ± 0.05	10^7−10^8
STD	none	12.1 ± 0.3	2.1 ± 1.1	0.19 ± 0.01	10^7−10^8

[a]Those of STD device are also listed for comparison. Average value and standard deviation are calculated from three individual devices.

Information). Hence, to improve the reproducibility of the proposed device, aligned nanowires produced by the spin coating method are used in the following works.

It is noted that the spin-coated nanowires form a radiative pattern on the substrate due to the centrifugal force. We define the nanowire orientation by choosing devices on different positions on the substrate (see Figure S1, Supporting Information). In future development, the nanowire alignment can be performed using nanoimprint,[23] nanowire electrospinning,[24] or nanowire contact coating[25] technologies. Here, in this work, choosing devices on radiative nanowire pattern enables us to quickly evaluate the performance of devices with aligned nanowires. As shown in the SEM images of Figure 3a, 3b, and 3c, with a controlled shield ratio around 10.5 ± 1.5%, the angle between the nanowire orientation and the current flow direction can be roughly determined as 90°, 45°, and 10°, respectively, where the corresponding transfer characteristics of AgO_xNW a-IGZO TFTs are shown in Figure 3d, 3e, and 3f. Reducing the angle between the nanowire orientation and current flow direction from 90° to 45° to 10° significantly increases the effective μ_{FE} from 28.3 to 70.8 to 105.3 cm^2/V s, respectively. To confirm the influence of nanowire orientation on device performance, three devices are independently characterized for each orientation condition. Their transfer characteristics are shown in Figure S4a−c, Supporting Information. With a fixed shield ratio of around 10.5%, similar device performance can be obtained when the nanowire orientation is controlled. The statistics of typical parameters, such as the effective mobility, threshold voltage, subthreshold swing, and on/off current ratio, are extracted from Figure S4, Supporting Information, and summarized in Table 1. Data from STD device are also listed. For devices with 90°, 45°, and 10° nanowire orientations, the average effective μ_{FE} with standard deviation is 26.7 ± 4.0, 76.8 ± 6.8, and 114.3 ± 10.2 cm^2/V s, respectively. Changing the nanowire orientation does not significantly influence the threshold voltage, subthreshold swing, and off-state current.

The increased effective μ_{FE} in AgO_xNW a-IGZO TFTs presumably results from the fact that silver nanowires can serve as highly conductive bus lines for electron transport from source to drain.[13,14] During the on state, gate bias enables injection of electrons into the active layer to form the channel with high-density electrons in the front interface of IGZO. With a lateral field, electrons travel through a-IGZO film with silver nanowires, inject into the metallic nanowires, and then exit to get into a-IGZO repeatedly. Silver nanowires reduce the effective channel length and therefore increase the "effective" μ_{FE}. It is noted that the effective μ_{FE} is extracted from the device current−voltage relationship by considering that the channel length is fixed as the distance between the source and the drain electrodes.[14] As a result, when the orientation of AgNWs is aligned with the current flow direction electrons can fully exploit the parallel conductive paths and the transistor delivers the largest output current drive. During the off state, on the other hand, gate bias impedes electron injection and depletes the IGZO active layer. Hence, there is no channel formation inside the IGZO region. The depleted IGZO regions disconnect electron transport from one nanowire to the other, hence leading to a low off-state current. If nanowire density is very high to form a conductive network, the depleted IGZO regions fail to disconnect nanowires and a short circuit current between source and drain will be observed. The influence of nanowire density (i.e., shield ratio) on μ_{FE} is further investigated by comparing μ_{FE} of 10°-aligned AgO_xNW a-IGZO TFTs with different shield ratios. As shown in Figure S4d, Supporting Information, when the shield ratio is as low as 3%, the effective μ_{FE} is almost the same as that in the STD device. Increasing the shield ratio to be around 4.5% can deliver effective μ_{FE} as 12−29 cm^2/V s. When the shield ratio increases to 10.5%, a high effective μ_{FE} with average value as 114.3 cm^2/V s and standard deviation as 10.2 can be obtained. In this study, the nanowire length is 10−20 μm and the alignment is not very well ordered. Hence, a large device-to-device deviation is observed. To avoid a short, a long channel length (500 μm) is also used to produce the transistors. In real applications, large pixel with low-cost shadow mask patterning may be used when developing transparent circuitry on window glass such as smart window technology. For other applications including display application or wearable flexible electronics, it is required to scale down the nanowire length as well as the channel length. Since the mechanism to obtain a high effective μ_{FE} is to introduce conductive bus lines to speed up the overall channel conduction, it is hence expected that a high effective μ_{FE} can be obtained when we scale down the nanowire length together with the channel length. In future work, nanotechnologies such as nanoimprint,[23] nanowire electrospinning,[24] and nanowire contact printing[25] are promising methods to realize AgO_xNW a-IGZO TFTs with scaled channel length and suppressed device-to-device deviation.

The subthreshold swing in Table 1 can be used to evaluate the interface trap state density (N_t)[29−32] according to

$$N_t = \left[\frac{S.S. \times \log(e)}{kT/q}\right]\frac{C_i}{q} \quad (1)$$

where C_i is the gate capacitance. The extracted N_t values with standard deviations are shown in Table 2. For all devices including STD controls and AgO_xNW a-IGZO TFTs with different nanowire orientations, the average N_t values are around 5.6−8.4 × 10^{11} cm^{-2}. Such N_t values are comparable to the N_t values in previous reports.[29−32] Even though the average N_t value slightly increases when reducing the nanowire orientation, such a slight variation is within the standard deviation due to the device-to-device variation. Also, no significantly different N_t values can be found between STD and AgO_xNW a-IGZO TFTs, indicating that adding nanowires into the active channel does not deteriorate the interface property.

DOI: 10.1021/am5059316
ACS Appl. Mater. Interfaces 2015, 7, 232−240

Table 2. On Voltages (V_{on}), Interface State Densities (N_t), and Channel Carrier Concentrations (N_{ch}) of AgO_xNW a-IGZO TFTs with Different Nanowire Orientations[a]

	nanowire orientation	V_{on} (V)	N_t	N_{ch}
AgO_xNW a-IGZO TFT	90°	−1	$(5.6 \pm 1.1) \times 10^{11}$	-6.6×10^{16}
	45°	−1	$(7.3 \pm 3.3) \times 10^{11}$	-6.6×10^{16}
	10°	−2	$(8.4 \pm 2.8) \times 10^{11}$	-1.3×10^{17}
STD	none	0.5	$(7.3 \pm 0.5) \times 10^{11}$	3.3×10^{16}

[a]Those of STD device are also listed for comparison.

Comparing STD IGZO TFT and AgO_xNW a-IGZO TFT we also found that AgO_xNW a-IGZO TFT exhibits a slight negatively shift threshold voltage. The negative shift threshold voltage in AgO_xNW a-IGZO TFTs indicates the increase of channel electron concentration. According to previous work,[33] when increasing the channel electron concentration in IGZO TFT a more negative threshold voltage is required to deplete the channel and turn off the transistor. The channel carrier concentration (N_{ch})[30,34] can be estimated using

$$N_{ch} = \frac{C_i V_{on}}{q t_c} \quad (2)$$

where V_{on} and t_c are the turn-on voltage and channel thickness. V_{on} and calculated N_{ch} are listed in Table 2. The positive N_{ch} value for STD device represents an enhancement-mode transistor in which the channel region is depleted under zero gate bias. Applying positive gate bias then enables electron injection from the source electrode to form the channel. The negative N_{ch} values for AgO_xNW a-IGZO TFTs, on the other hand, indicate the existence of channel electrons at zero gate bias. Adding conductive AgO_x nanowires into the IGZO channel increases the channel electron concentration and hence shifts the threshold voltage to be around 0.2−0.7 V. The close-to-zero threshold voltage ensures low-power operation.

Then, to examine the microstructure and compositions between a-IGZO and AgNW, high-resolution TEM integrated with energy-dispersive spectroscopy (EDS) was performed. Figure 4a shows a cross-sectional TEM image of an IGZO/AgNW film, while Figure 4b shows a magnified image of the AgNW taken from Figure 4a. The morphology of the AgNW embedded in the a-IGZO film was clearly observed. We note that the cracks found in the a-IGZO film surrounding the nanowire were most likely induced during preparation of TEM samples using focused ion beam (FIB) cutting. The TEM image with corresponding EDS element profile is shown in Figure S5, Supporting Information. As summarized in Table 3, the corresponding chemical compositions of the IGZO at position a were quantitatively measured to be 19.7 atom % In, 22.3 atom % Ga, 11.2 atom % Zn, and 46.8 atom % O, while the chemical compositions of the AgNW at positions b and c are similar, measured to be ∼73.6 atom % Ag, ∼2.6 atom % In, and ∼25.4 atom % O. Interestingly, ∼2.6 atom % In and ∼25.4 atom % O at positions b and c in AgNW indicate an evident diffusion of In and O atoms deep into AgNWs during the thermal annealing process. The high-resolution TEM image shown in Figure 4c also indicates a single-crystalline feature where the internal plane spacings of 0.25 and 0.2 nm were indexed, which match with the (100) and (103) planes. In our previous work, the diffusion and oxidation of Ca in a-IGZO enhanced the effective mobility in a-IGZO TFT.[35] Here, in this

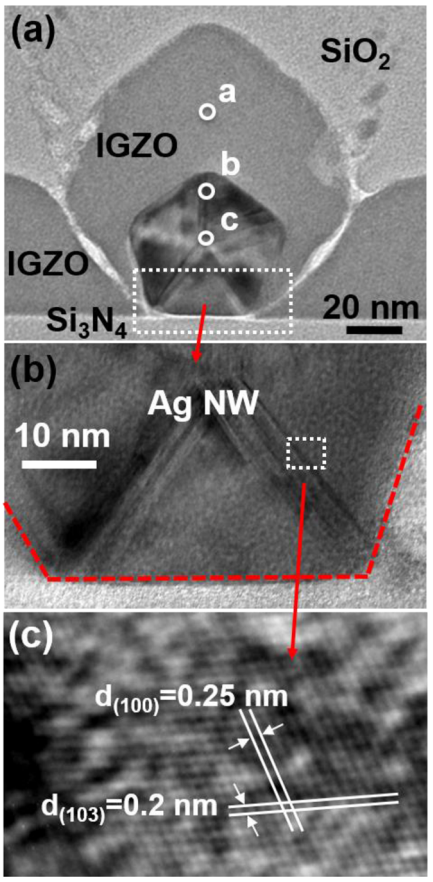

Figure 4. (a and b) TEM and (c) EDS image of the IGZO-covered nanowire in AgO_xNW a-IGZO TFT.

Table 3. Quantitative Elemental Compositions Measured from TEM/EDS as Marked in Figure 4a

no.	Ag (atom %)	In (atom %)	Ga (atom %)	Zn (atom %)	O (atom %)	total (atom %)
a		19.7	22.3	11.2	46.8	100
b	73.6	3			25.4	100
c	72.2	2.2			25.6	100

work, TEM and EDS analyses reveal that the silver nanowire becomes an AgO_x (with 2−3% In) metal oxide compound after room-temperature IGZO sputtering and 400 °C thermal annealing in the nitrogen furnace.

As it appears that AgO_x instead of Ag nanowires contributes to the excellent device performance, we aim to understand the interaction between silver nanowires and a-IGZO under similar process conditions. First, we try to check the conductivity of the AgO_x nanowires. A two-terminal AgO_x-nanowires resistance is formed by covering AgNW with room-temperature sputtered IGZO with 400 °C postannealing. The electrical property of the two-terminal device is shown in Figure S6, Supporting Information. A small sheet resistance as 148 kΩ is obtained, verifying good conductivity in the mixed material. Since IGZO is a semiconductor material it is proposed that the AgO_x nanowires are conductive nanowires. Next, we survey if the IGZO film serves as a passivation over AgNW. Many studies have suggested that silver nanowires can be easily oxidized in air;[36,37] passivation methods such as reduced graphene oxide[38] or indium-doped zinc oxide (IZO) buffer layer capping[37] have been proposed to suppress oxidation on

DOI: 10.1021/am5059316
ACS Appl. Mater. Interfaces 2015, 7, 232−240

the surface of silver nanowires. It is therefore of great interest to investigate whether the a-IGZO film plays a passivation role over silver nanowires and has a positive impact on the device performance. A series of experiments has been conducted to examine the possibility. We first perform a 400 °C annealing in nitrogen on the substrate coated with AgNWs prior to a-IGZO deposition. A previous report has shown that silver nanowires melt to form small droplets at an annealing temperature as low as 300 °C.[39] The AgO_xNW a-IGZO TFT with such a 400 °C preannealing process exhibits a low mobility of 9.7 cm^2/V s, which is similar to the STD device. An AFM image verifies that silver nanowires are self-assembled into small clusters after 400 °C preannealing (see Figure S7, Supporting Information), eliminating the advantage of having embedded conductive paths within a-IGZO. Detailed device characteristics are provided in the Supporting Information.

We next change the substrate temperature during RF sputtering of a-IGZO, which is also referred to as the sputtering temperature, to investigate the impact on the performance of AgO_xNW a-IGZO TFTs. Detailed transfer characteristics and extracted typical parameters are provided in the Supporting Information (see Figure S8 and Table S1). The effective mobility as a function of sputtering temperature is plotted in Figure 5a. Increasing the substrate temperature significantly

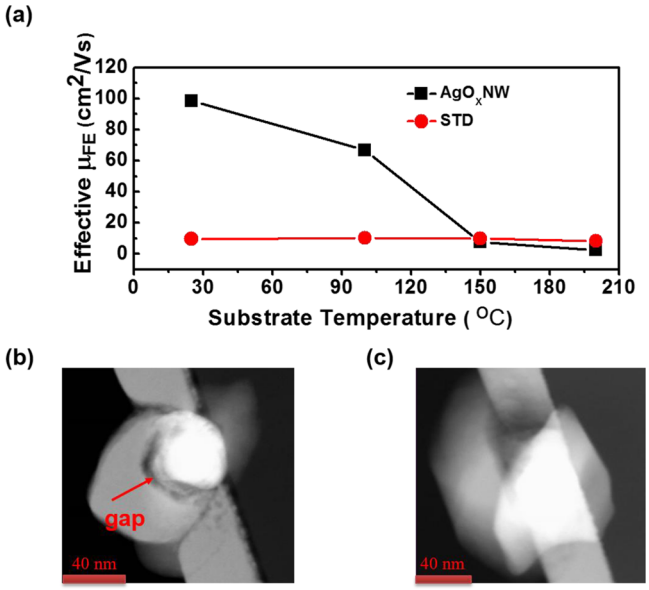

Figure 5. (a) Effective field-effect mobility of AgO_xNW a-IGZO TFT as a function of sputtering temperature. Sputtering temperature is the substrate temperature during IGZO RF sputtering. (b and c) TEM images of two separate nanowires on the sample with 150 °C sputtering temperature.

deteriorates the performance of AgO_xNW a-IGZO TFT. When the substrate temperature is higher than 100 °C, the effective mobility of AgO_xNW a-IGZO TFTs is even lower than that of a STD a-IGZO TFT. Low-temperature (<100 °C) sputtering of a-IGZO is necessary to obtain good performance in AgO_xNW a-IGZO TFT. Since the sputtering temperature does not significantly affect the mobility of STD a-IGZO TFTs (see Table S2, Supporting Information) nor the distribution of nanowires (see SEM image in Figure S9, Supporting Information, no melting is observed), we suspect that the sputtering temperature may change the IGZO/nanowire interface. Two silver nanowire samples covered by 150 °C sputtered IGZO film (with 400 °C postannealing) were analyzed using high-angle annular dark field (HAADF) TEM with the corresponding EDS analysis. HAADF TEM images of the two nanowire samples are shown in Figure 5b and 5c. The corresponding EDS mapping images of the two samples (with identical process condition) are shown in Figures S10 and S11, Supporting Information. A gap between IGZO and nanowire is clearly observed in Figure 5b. In Figure 5c the nanowire even loses its pentagon cross-sectional shape, indicating that the nanowire morphology is destroyed. The gap between the nanowire and the IGZO film or the destroyed nanowire morphology will lead to electrical disconnect between IGZO and nanowire. Hence, we proposed that the poor mobility in AgO_xNW a-IGZO TFT with 150 °C sputtering temperature is due to the poor contact between IGZO and nanowires and hence the loss of bus line effect. When the nanowires no longer act as high-speed bus lines they may become scattering centers to impede electron transport. Hence, the effective mobility is even smaller than that in the STD device. When increasing the sputtering temperature, the IGZO metal ion diffusion behavior is also enhanced. The EDS mapping images in Figures S10 and S11, Supporting Information, tell that when sputtering IGZO film on AgNW with 150 °C sputtering temperature the indium, zinc and gallium signals are found inside the nanowire region. This result is different from the EDS analysis on room-temperature sputtered IGZO on AgNW (Figure S5, Supporting Information), in which only indium diffusion is observed inside the nanowire regions. Finally, the silver diffusion behavior is also influenced by increasing sputtering temperature. With room-temperature IGZO sputtering, silver signal is mostly confined inside the nanowire regions (see Figure S5, Supporting Information). With 150 °C sputtered IGZO, however, an obvious silver signal is found in the nitride layer to reveal the severe silver diffusion into the underlying gate insulating film. The severe diffusion of indium, gallium, and zinc into the nanowire or silver diffusion into the gate insulator, however, may not explain the low effective μ_{FE} directly. In the future, more detailed material analysis should be performed to further understand the relationship between metal diffusion and nanowire morphology. Here, destruction of nanowire morphology and hence the poor contact between IGZO and nanowires are proposed to explain the poor effective μ_{FE} in AgO_xNW a-IGZO TFT with elevated sputtering temperature.

Even though we found that the good contact between IGZO and nanowire is the key to obtain a high effective μ_{FE}, the contact is found to exhibit a small potential barrier to limit electron transport at low lateral field (drain bias). As shown in Figure 6a we compare the effective μ_{FE} of a STD and an AgO_xNW a-IGZO TFT at different drain biases. For V_D = 0.1, 1, and 5 V, the effective mobility is extracted from linear-region transconductance. For V_D = 20 V, saturation-region transconductance at V_G = 18 V is used to extract the effective mobility in the saturation region. It is observed that μ_{FE} in the STD a-IGZO TFT keeps almost the same when drain bias changes from 0.1 to 20 V. This is reasonable since the intrinsic mobility should not depend on the lateral field in the low-field regime. For the AgO_xNW a-IGZO TFT, however, the effective μ_{FE} significantly increases with increasing drain bias. The output characteristics of AgO_xNW a-IGZO TFT are shown in Figure 6b. The comparison of the output curves, transfer curves, and transconductance curves of STD and AgO_xNW a-IGZO TFT are shown in Figure S12, Supporting Information. The mobility

DOI: 10.1021/am5059316
ACS Appl. Mater. Interfaces 2015, 7, 232−240

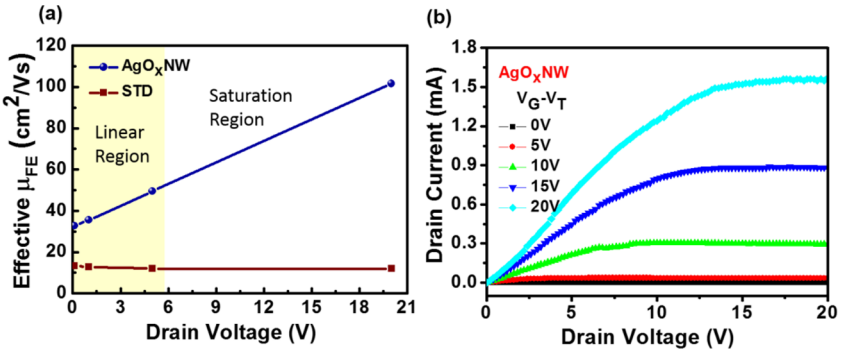

Figure 6. (a) Effective field-effect mobility plotted as a function of drain voltage for STD and AgO$_x$NW a-IGZO TFTs. (b) Output characteristics of AgO$_x$NW a-IGZO TFT.

calculation is listed in Table S3, Supporting Information. The saturation behavior of AgO$_x$NW a-IGZO TFT is slightly inferior to that of the STD device. Such a property does not limit its future development because linear-region-operated transistors can be used in many applications including the pixel circuitry in liquid-crystal display. As discussed previously, the effective mobility of AgO$_x$NW a-IGZO TFTs should be monotonically proportional to the ratio of nanowire conduction over the conduction through pristine a-IGZO. At low drain bias, the relatively low effective μ_{FE} indicates that electron transport through a-IGZO/nanowire interface is suppressed. We proposed that an energy barrier is formed at a-IGZO/nanowire interface to impede the electron transport at low electric field. From source to drain multiple a-IGZO/nanowire interfaces represent multiple energy barriers on the conduction band. The phenomenon is analogous to polycrystalline silicon (Poly-Si) TFTs, where the energy barrier at grain boundaries also creates such a multiple-barrier conduction band. Drain-induced grain barrier lowering is a known mechanism which significantly influences the effective mobility in Poly-Si TFTs.[40,41] In our previous works on a-IGZO TFTs with nanometer dot-like doping, a field-induced barrier lowering effect is also observed.[42,43] Here, drain-induced interface barrier lowering is proposed to explain the results shown in Figure 6a. An energy barrier at the a-IGZO/nanowire interface impedes electron transport at low drain bias. Increasing drain bias can effectively lower down the energy barrier, enhance electron transport through the a-IGZO/nanowire matrix, and then increase the effective μ_{FE}.

The hysteresis, bias-stress reliability, and lifetime of the AgO$_x$NW a-IGZO TFT are then investigated. The hysteresis behavior of STD and AgO$_x$NW a-IGZO TFTs is compared in Figure S13a, Supporting Information. There is no obvious hysteresis effect in both devices. The transfer curves of STD and AgO$_x$NW a-IGZO TFTs under bias stress are shown in Figure S13b, Supporting Information. The stress condition is $V_G - V_T = 20$ V and $V_D = V_S = 0$ V. The threshold voltage shift in two devices is plotted as a function of stress time in Figure S13c, Supporting Information. Threshold voltage shift is defined as the threshold voltage after stress minus the original threshold voltage before stress. It is noted that both STD and AgO$_x$NW a-IGZO TFTs are unpassivated. Hence, a large positive shift in the threshold voltage is observed because the ambient oxygen and water molecules enter IGZO bulk to enhance defect generation and electron trapping.[44] AgO$_x$NW a-IGZO TFT and STD IGZO TFT, however, exhibit similar threshold voltage shifts during the stress. These results suggest that adding AgO$_x$NW into the IGZO channel will not significantly cause a hysteresis effect nor degrade the bias-stress reliability.

Finally, AgNW a-IGZO TFTs demonstrate extraordinary lifetime. We track the transfer characteristics of an AgNW a-IGZO TFT for over 93 days (see Figure S14, Supporting Information), where the typical parameters such as effective μ_{FE}, threshold voltage shift, subthreshold swing, and off-state current (I_{off}) are plotted as a function of storage time as shown in Figure 7. Since there is no additional passivation layer above

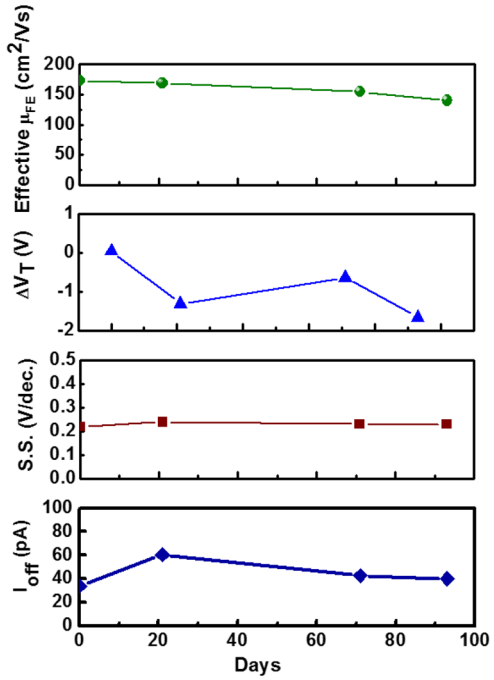

Figure 7. Effective field-effect mobility, threshold voltage shift, subthreshold swing, and off-state current (I_{off}) of AgO$_x$NW a-IGZO TFT tracked as a function of storage day in the air ambient.

the a-IGZO film and the device is stored in the air ambient (with relative humidity lower than 55%). The initial effective μ_{FE} is as high as 174 cm^2/V s. The highest effective μ_{FE} is obtained by controlling the angle between the nanowire orientation and the current flow to be almost parallel and the shield ratio as high as 15%. After being stored in air for 21 days, the effective μ_{FE} slightly degrades to be 169 cm^2/V s. After 93 days, μ_{FE} as high as 140 cm^2/V s is still obtained. The excellent lifetime in AgNW a-IGZO TFT not only verifies the robust

DOI: 10.1021/am5059316
ACS Appl. Mater. Interfaces 2015, 7, 232−240

conductive nanowire system but also makes AgNW a-IGZO TFT a promising candidate for future ultralow power device applications.

CONCLUSION

In summary, we demonstrated a very high effective μ_{FE} (100−174 cm^2/V s) in sputtered a-IGZO TFTs by introducing silver nanowires into the active region. According to the TEM/EDS analyses it is found that silver nanowires have become robust AgO_x compounds after room-temperature sputtering of a-IGZO followed by 400 °C annealing in the nitrogen ambient. The conductive AgO_x nanowires serve as bus lines to speed up the carrier transport from source to drain. Consequently, controlling the orientation of $InAgO_x$ nanowires significantly affects the effective mobility. Maximum mobility can be obtained when the orientation of $InAgO_x$ nanowires is in parallel with the direction of current flow. The unchanged morphology of the conductive AgO_x nanowires and the good contact between IGZO and nanowires are critical to achieve a high effective field-effect mobility. If the sputtering temperature is increased to destroy the contact between nanowire and IGZO film, the effective field-effect mobility seriously degrades to be as low as 2.4 cm^2/V s. Using room-temperature sputtering with a following 400 °C annealing facilitates formation of a robust conductive nanowire system in AgO_xNW a-IGZO TFTs, giving rise to excellent device reliability with no hysteresis and a lifetime for over 93 days.

ASSOCIATED CONTENT

Supporting Information

Process schematic to obtain AgO_xNW a-IGZO TFTs with different orientations; AFM image of an AgO_xNW a-IGZO TFT that underwent 400 °C preannealing; extracted typical parameters of AgO_xNW and STD a-IGZO TFTs with different sputtering temperatures; TEM/EDS analysis for AgO_xNW a-IGZO TFT with elevated sputtering temperature; hysteresis and bias stress reliability measurement data; and transfer characteristics for an AgO_xNW a-IGZO TFT tracked for 93 days. This material is available free of charge via the Internet at http://pubs.acs.org.

AUTHOR INFORMATION

Corresponding Authors

*E-mail: hsiaowen@mail.nctu.edu.tw.
*E-mail: yup@faculty.nctu.edu.tw.

Notes

The authors declare no competing financial interest.

ACKNOWLEDGMENTS

The authors thank the Ministry of Science and Technology in Taiwan for financial support under grant nos. 101-2221-E-009-051-MY2 and 100-2628-E-009-020-MY3. This work was also partially supported by E-ink Holdings Inc.

REFERENCES

(1) Nomura, K.; Ohta, H.; Takagi, A.; Kamiya, T.; Hirano, M.; Hosono, H. Room-Temperature Fabrication of Transparent Flexible Thin-Film Transistors Using Amorphous Oxide Semiconductors. *Nature* **2004**, *432*, 488−492.

(2) Yabuta, H.; Sano, M.; Abe, K.; Aiba, T.; Den, T.; Kumomi, H.; Nomura, K.; Kamiya, T.; Hosono, H. High-Mobility Thin-Film Transistor with Amorphous InGaZnO4 Channel Fabricated by Room Temperature Rf-Magnetron Sputtering. *Appl. Phys. Lett.* **2006**, *89*, 112123.

(3) Banger, K. K.; Yamashita, Y.; Mori, K.; Peterson, R. L.; Leedham, T.; Rickard, J.; Sirringhaus, H. Low-Temperature, High-Performance Solution-Processed Metal Oxide Thin-Film Transistors Formed by a 'Sol−Gel on Chip' Process. *Nat. Mater.* **2011**, *10*, 45−50.

(4) Hosono, H. Ionic Amorphous Oxide Semiconductors: Material Design, Carrier Transport, and Device Application. *J. Non-Cryst. Solids* **2006**, *352*, 851−858.

(5) Yu, X.; Zhou, N.; Smith, J.; Lin, H.; Stallings, K.; Yu, J.; Marks, T. J.; Facchetti, A. Synergistic Approach to High-Performance Oxide Thin Film Transistors Using a Bilayer Channel Architecture. *ACS Appl. Mater. Interfaces* **2013**, *5*, 7983−7988.

(6) Lee, J. E.; Sharma, B. K.; Lee, S.-K.; Jeon, H.; Hong, B. H.; Lee, H.-J.; Ahn, J.-H. Thermal Stability of Metal Ohmic Contacts in Indium Gallium Zinc Oxide Transistors Using a Graphene Barrier Layer. *Appl. Phys. Lett.* **2013**, *102*, 113112.

(7) Yu, S. H.; Kim, B. J.; Kang, M. S.; Kim, S. H.; Han, J. H.; Lee, J. Y.; Cho, J. H. In/Ga-Free, Inkjet-Printed Charge Transfer Doping for Solution-Processed ZnO. *ACS Appl. Mater. Interfaces* **2013**, *5*, 9765−9769.

(8) Qian, L. X.; Lai, P. T. Fluorinated InGaZnO Thin-Film Transistor with HfLaO Gate Dielectric. *IEEE Electron Device Lett.* **2014**, *35*, 363−365.

(9) Zhou, J.; Wu, G.; Guo, L.; Zhu, L.; Wan, Q. Flexible Transparent Junctionless TFTs with Oxygen-Tuned Indium-Zinc-Oxide Channels. *IEEE Electron Device Lett.* **2013**, *34*, 888−890.

(10) Hsu, H.-H.; Chang, C.-Y.; Cheng, C.-H. A Flexible IGZO Thin-Film Transistor with Stacked TiO_2-Based Dielectrics Fabricated at Room Temperature. *IEEE Electron Device Lett.* **2013**, *34*, 768−770.

(11) Lee, M.-S.; Lee, K.; Kim, S.-Y.; Lee, H.; Park, J.; Choi, K.-H.; Kim, H.-K.; Kim, D.-G.; Lee, D.-Y.; Nam, S. W.; et al. High-Performance, Transparent, and Stretchable Electrodes Using Graphene−Metal Nanowire Hybrid Structures. *Nano Lett.* **2013**, *13*, 2814−2821.

(12) Wang, C. L.; Liu, X. Q.; Xiao, X. H.; Liu, Y. L.; Chen, W.; Li, J. C.; Shen, G. Z.; Liao, L. High-Mobility Solution-Processed Amorphous Indium Zinc Oxide/In_2O_3 Nanocrystal Hybrid Thin-Film Transistor. *IEEE Electron Device Lett.* **2013**, *34*, 72−74.

(13) Liu, X.; Wang, C.; Cai, B.; Xiao, X.; Guo, S.; Fan, Z.; Li, J.; Duan, X.; Liao, L. Rational Design of Amorphous Indium Zinc Oxide/Carbon Nanotube Hybrid Film for Unique Performance Transistors. *Nano Lett.* **2012**, *12*, 3596−3601.

(14) Liu, X.; Wang, C.; Xiao, X.; Wang, J.; Guo, S.; Jiang, C.; Yu, W. J.; Hu, W.; Li, J.; Liao, L. High Mobility Amorphous InGaZnO Thin Film Transistor with Single Wall Carbon Nanotubes Enhanced-Current Path. *Appl. Phys. Lett.* **2013**, *103*, 223108.

(15) Kang, N.; Sarker, B. K.; Khondaker, S. I. The Effect of Carbon Nanotube/Organic Semiconductor Interfacial Area on the Performance of Organic Transistors. *Appl. Phys. Lett.* **2012**, *101*, 233302.

(16) Liu, X.; Jiang, L.; Zou, X.; Xiao, X.; Guo, S.; Jiang, C.; Liu, X.; Fan, Z.; Hu, W.; Chen, X.; et al. Scalable Integration of Indium Zinc Oxide/Photosensitive-Nanowire Composite Thin-Film Transistors for Transparent Multicolor Photodetectors Array. *Adv. Mater.* **2014**, *26*, 2919−2924.

(17) Lee, M.-J.; Lee, T. I.; Park, J. H.; Kim, J. H.; Chae, G. S.; Jun, M. C.; Hwang, Y. K.; Baik, H. K.; Lee, W.; Myoung, J.-M. Modulation of the Operational Characteristics of Amorphous In−Ga−Zn−O Thin-Film Transistors by In_2O_3 Nanoparticles. *J. Phys. D: Appl. Phys.* **2012**, *45*, 205303.

(18) Hu, L.; Kim, H. S.; Lee, J.-Y.; Peumans, P.; Cui, Y. Scalable Coating and Properties of Transparent, Flexible, Silver Nanowire Electrodes. *ACS Nano* **2010**, *4*, 2955−2963.

(19) Ni, C.; Hassan, P. A.; Kaler, E. W. Structural Characteristics and Growth of Pentagonal Silver Nanorods Prepared by a Surfactant Method. *Langmuir* **2005**, *21*, 3334−3337.

(20) Liu, C.-H.; Yu, X. Silver Nanowire-Based Transparent, Flexible, and Conductive Thin Film. *Nanoscale Res. Lett.* **2011**, *6*, 75.

DOI: 10.1021/am5059316
ACS Appl. Mater. Interfaces 2015, 7, 232−240

(21) Garnett, E. C.; Cai, W.; Cha, J. J.; Mahmood, F.; Connor, S. T.; Christoforo, M. G.; Cui, Y.; McGehee, M. D.; Brongersma, M. L. Self-Limited Plasmonic Welding of Silver Nanowire Junctions. *Nat. Mater.* **2012**, *11*, 241−249.
(22) Yang, L.; Zhang, T.; Zhou, H.; Price, S. C.; Wiley, B. J.; You, W. Solution-Processed Flexible Polymer Solar Cells with Silver Nanowire Electrodes. *ACS Appl. Mater. Interfaces* **2011**, *3*, 4075−4084.
(23) Wang, J. J.; Chen, L.; Liu, X.; Sciortino, P.; Liu, F.; Walters, F.; Deng, X. 30-nm-Wide Aluminum Nanowire Grid for Ultrahigh Contrast and Transmittance Polarizers made by UV-Nanoimprint Lithography. *Appl. Phys. Lett.* **2006**, *89*, 141105.
(24) Chen, J.-Y.; Wu, H.-C.; Chiu, Y.-C.; Chen, W.-C. Plasmon-Enhanced Polymer Photovoltaic Device Performance Using Different Patterned Ag/PVP Electrospun Nanofibers. *Adv. Energy Mater.* **2014**, *4*, 1301665.
(25) Liu, X.; Long, Y.-Z.; Liao, L.; Duan, X.; Fan, Z. Large-Scale Integration of Semiconductor Nanowires for High-Performance Flexible Electronics. *ACS Nano* **2012**, *6*, 1888−1900.
(26) Dan, B.; Irvin, G. C.; Pasquali, M. Continuous and Scalable Fabrication of Transparent Conducting Carbon Nanotube Films. *ACS Nano* **2009**, *3*, 835−843.
(27) Aoi, T.; Oka, N.; Sato, Y.; Hayashi, R.; Kumomi, H.; Shigesato, Y. DC Sputter Deposition of Amorphous Indium−Gallium−Zinc−Oxide (a-IGZO) Films with H2O Introduction. *Thin Solid Films* **2010**, *518*, 3004−3007.
(28) Zan, H. W.; Chen, W. T.; Hsueh, H. W.; Kao, S. C.; Ku, M. C.; Tsai, C. C.; Meng, H. F. Amorphous Indium-Gallium-Zinc-Oxide Visible-Light Phototransistor with a Polymeric Light Absorption Layer. *Appl. Phys. Lett.* **2010**, *97*, 203506.
(29) Jeong, J. K.; Jeong, J. H.; Yang, H. W.; Park, J. S.; Mo, Y. G.; Kim, H. D. High Performance Thin Film Transistors with Cosputtered Amorphous Indium Gallium Zinc Oxide Channel. *Appl. Phys. Lett.* **2007**, *91*, 113505.
(30) Kim, C. E.; Cho, E. N.; Moon, P.; Kim, G. H.; Kim, D. L.; Kim, H. J.; Yun, I. Density-of-States Modeling of Solution-Processed InGaZnO Thin-Film Transistors. *IEEE Electron Device Lett.* **2010**, *31*, 1131−1133.
(31) Chang, S.-J.; Chang, T. H.; Weng, W. Y.; Chiu, C. J.; Chang, S. P. Amorphous InGaZnO Ultraviolet Phototransistors With a Thin Ga2O3 Layer. *IEEE J. Sel. Top. Quantum Electron.* **2014**, *20*, 1−5.
(32) Kagan, C. Y.; Andry, P. W. E. *Thin Film Transistors*; Dekker Publications: New York, 2003; p 87.
(33) Park, J.-S.; Jeong, J. K.; Mo, Y.-G.; Kim, H. D.; Kim, C.-J. Control of Threshold Voltage in ZnO-Based Oxide Thin Film Transistors. *Appl. Phys. Lett.* **2008**, *93*, 033513.
(34) Dehuff, N. L.; Kettenring, E. S.; Hong, D.; Chiang, H. Q.; Wager, J. F.; Hoffman, R. L.; Park, C.-H.; Keszler, D. A. Transparent Thin-Film Transistors with Zinc Indium Oxide Channel Layer. *J. Appl. Phys.* **2005**, *97*, 064505.
(35) Zan, H.-W.; Yeh, C.-C.; Meng, H.-F.; Tsai, C.-C.; Chen, L.-H. Achieving High Field-Effect Mobility in Amorphous Indium-Gallium-Zinc Oxide by Capping a Strong Reduction Layer. *Adv. Mater.* **2012**, *24*, 3509−3514.
(36) Tsai, Y.-J.; Chang, C.-Y.; Lai, Y.-C.; Yu, P.-C.; Ahn, H. Realization of Metal−Insulator Transition and Oxidation in Silver Nanowire Percolating Networks by Terahertz Reflection Spectroscopy. *ACS Appl. Mater. Interfaces* **2014**, *6*, 630−635.
(37) Lee, H. J.; Hwang, J. H.; Choi, K. B.; Jung, S.-G.; Kim, K. N.; Shim, Y. S.; Park, C. H.; Park, Y. W.; Ju, B.-K. Effective Indium-Doped Zinc Oxide Buffer Layer on Silver Nanowires for Electrically Highly Stable, Flexible, Transparent, and Conductive Composite Electrodes. *ACS Appl. Mater. Interfaces* **2013**, *5*, 10397−10403.
(38) Ahn, Y.; Jeong, Y.; Lee, Y. Improved Thermal Oxidation Stability of Solution-Processable Silver Nanowire Transparent Electrode by Reduced Graphene Oxide. *ACS Appl. Mater. Interfaces* **2012**, *4*, 6410−6414.
(39) Madaria, A. R.; Kumar, A.; Ishikawa, F. N.; Zhou, C. Uniform, Highly Conductive, and Patterned Transparent Films of a Percolating Silver Nanowire Network on Rigid and Flexible Substrates Using a Dry Transfer Technique. *Nano Res.* **2010**, *3*, 564−573.
(40) Lin, P. S.; Guo, J. Y.; Wu, C. Y. A Quasi-Two-Dimensional Analytical Model for the Turn-On Characteristics of Polysilicon Thin-Film Transistors. *IEEE Electron Device Lett.* **1990**, *37*, 666−674.
(41) Hsiao, Y.-H.; Lue, H.-T.; Chen, W.-C.; Chen, C.-P.; Chang, K.-P.; Shih, Y.-H.; Tsui, B.-Y.; Lu, C.-Y. Modeling the Variability Caused by Random Grain Boundary and Trap-location Induced Asymmetrical Read Behavior for a Tight-pitch Vertical Gate 3D NAND Flash Memory Using Double-Gate Thin-Film Transistor (TFT) Device. *Proc. IEEE Int. Electron Devices Meeting (IEDM)* **2012**, *12*, 609.
(42) Zan, H.-W.; Tsai, W.-W.; Chen, C.-H.; Tsai, C.-C. Effective Mobility Enhancement by Using Nanometer Dot Doping in Amorphous IGZO Thin-Film Transistors. *Adv. Mater.* **2011**, *23*, 4237−4242.
(43) Liao, C.-H.; Li, C.-H.; Zan, H.-W.; Meng, H.-F.; Tsai, C.-C. High-Current-Drive Dual-Gate a-IGZO TFT with Nanometer Dotlike Doping. *IEEE Electron Device Lett.* **2013**, *34*, 1274−1276.
(44) Choi, S.-H.; Jang, J.-H.; Kim, J.-J.; Han, M.-K. Low-Temperature Organic (CYTOP) Passivation for Improvement of Electric Characteristics and Reliability in IGZO TFTs. *IEEE Electron Device Lett.* **2012**, *33*, 381−383.

DOI: 10.1021/am5059316
ACS Appl. Mater. Interfaces 2015, 7, 232−240